Geotextiles and Geomembranes xxx (2015) 1–14

Contents lists available at ScienceDirect

Geotextiles and Geomembranes

journal homepage: www.elsevier.com/locate/geotexmem

Experimental study on performance of geosynthetic-reinforced soil model walls on rigid foundations subjected to static footing loading

Chengzhi Xiao [a], Jie Han [b, *], Zhen Zhang [c]

[a] School of Civil Engineering, Hebei University of Technology, Tianjin 300401, China
[b] Civil, Environmental, and Architectural Engineering (CEAE) Department, The University of Kansas, KS 66045, USA
[c] Key Laboratory of Geotechnical and Underground Engineering of Ministry of Education, and Department of Geotechnical Engineering, Tongji University, Shanghai 200092, China

ARTICLE INFO

Article history:
Received 14 December 2014
Received in revised form
3 May 2015
Accepted 2 June 2015
Available online xxx

Keywords:
Bearing capacity
Footing
Geosynthetic-reinforced soil
Slope stability
Wall

ABSTRACT

Geosynthetic-reinforced soil (GRS) walls have been increasingly used to support bridge foundations as abutment walls. On the GRS abutment wall, large footing loads are applied adjacent to the wall facing. However, so far limited studies have been conducted to investigate the performance of GRS abutment walls subjected to static or dynamic loading. This study presents a series of model tests on the GRS walls to evaluate the effects of several influence factors, including the offset distance of a strip footing, the width of the strip footing, the length of geogrid reinforcement, and the connection mode between geogrid and facing, on the ultimate bearing capacities of the strip footings on the GRS walls. The settlements of the loading plate and the lateral displacements of the wall facing during loading were monitored. Thin colored sand layers were placed in the backfill sand to observe possible failure surfaces developing in the GRS walls. The experimental results showed that the footings on the GRS walls with 0.7H (H is the wall height) long reinforcement reached the maximum bearing capacities at the offset distances of 0.3*H* and 0.4*H* in the wall tests with mechanical and frictional connections, respectively. When the GRS walls had the geogrids with longer reinforcement length (2H), the ultimate bearing capacity increased with the offset distance of the footing and became constant when the offset was greater than 0.4H. It was observed that the failure surface started from the edge of the footing and exited from the facing of the wall. Based on the limit equilibrium analyses, under the footing loading, the slip surfaces by Spencer's two-part wedge method had a good agreement with those observed in the model tests.

1. Introduction

Geosynthetics-reinforced soil (GRS) walls have been successfully used for many applications under static and dynamic loading (for example, Tatsuoka et al., 1997; Leshchinsky and Han, 2004; Berg et al., 2009; Ling et al., 2009; Han and Leshchinsky, 2010). In the recent years, GRS walls have been increasingly used to support bridge abutments (for example, Ketchart and Wu, 1997; Abu-Hejleh et al., 2000; Tatsuoka et al., 2009). Bridge abutments are often supported by pile foundations in GRS walls (Pierson et al., 2009, 2011; Huang et al., 2011, 2013, 2014). Recently, GRS walls with shallow footings are increasingly used to support bridge abutments. Fig. 1 illustrates a GRS bridge abutment on a shallow footing. On the GRS abutment wall, large footing loads are often applied close to the wall facing, which is different from the typical and traditional applications of GRS walls. GRS bridge abutment walls with shallow footings eliminate the use of pile foundations and reduce bridge bumps at the interface between an approaching embankment and a bridge. As a result, they create a more economic and safer solution (Koerner, 1996; Helwany et al., 2003). A few field GRS abutment walls have been constructed and demonstrated their excellent performance with small deformation and high load-carrying capacity (Adams, 1997; Abu-Hejleh et al., 2000).

One of the well-documented GRS abutment wall projects was a 6 m high GRS abutment constructed by the Colorado Department of Transportation at Founders/Meadows, Colorado, in the United States (Abu-Hejleh et al., 2001). After construction, a series of load tests were conducted to carefully investigate the performance of the earth structure. The tests showed satisfactory results with a 10 mm maximum lateral deformation of the wall facing and a

* Corresponding author.
E-mail address: jiehan@ku.edu (J. Han).

http://dx.doi.org/10.1016/j.geotexmem.2015.06.001
0266-1144/

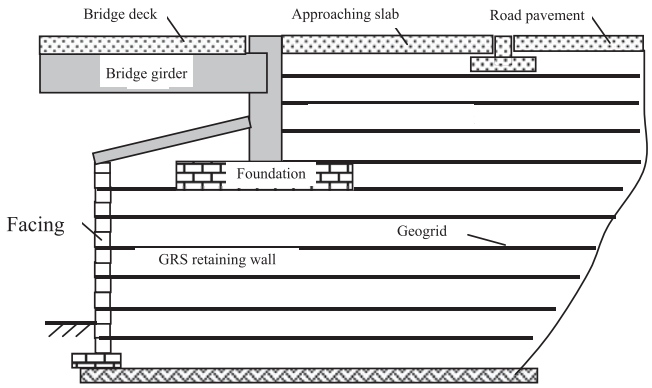

Fig. 1. Typical cross section of a GRS bridge abutment (modified from Abu-Hejleh et al., 2000).

14 mm settlement of the bridge footing. In addition, Adams and Collin (1997) and Ketchart and Wu (1997) carried out large or field loading tests on geosynthetic-reinforced foundations and GRS abutment walls. At the design pressure of 200 kPa, the GRS walls performed well (Elias et al., 2001). So far, the majority of GRS abutment walls have been founded on the competent foundations and they performed well under service loads. However, a few GRS walls have been constructed on relative weak foundations. Field test data and numerical analysis results also showed satisfactory performance of these walls despite the existence of the unfavorable foundation conditions (Wakai et al., 1996; Rowe and Skinner, 2001; Skinner and Rowe, 2005; Hara et al., 2004).

As compared with typical and traditional GRS walls, the GRS abutment walls are generally subjected to high footing loads that are close to the wall facing. Under such a condition, not only the stability of the GRS wall but also the bearing capacity and settlement of the bridge footing should be considered in design. The stability of the GRS wall is affected by the applied load through the footing. In addition to the magnitude of the load, the location or offset distance of the footing to the wall facing can affect the stability of the GRS wall, the bearing capacity as well as the settlement of the bridge foundation when the footing is located adjacent to the facing.

The interaction between the GRS wall and the footing is a complicated problem, which has not been well investigated. Wu et al. (2006) investigated the effect of bridge sill type, sill width, soil stiffness/strength, reinforcement spacing, and foundation stiffness on the load-carrying capacities of GRS abutment sills. Based on the limiting displacement and shear strain criteria, Wu et al. (2006) determined the allowable bearing pressures of the GRS abutments. Bourgeois et al. (2011) analyzed the mechanical response of earth structures reinforced with steel strips to traffic loads. El Sawwaf (2007) carried out a series of reduced-scale model tests to examine the behavior of strip footings on geogrid-reinforced sand over a soft clay slope. The test results indicated that the inclusion of geogrid layers in sand not only significantly improved the footing performance but also led to a great reduction in the depth of the reinforced sand layer required to achieve the allowable settlement. Bilgin (2009) investigated the effect of reinforcement length on the failure mechanism of GRS walls. Leshchinsky (2014) recently investigated the effects of footing location, reinforcement strength, and reinforcement spacing on the bearing capacity of the footing on the GRS wall and the failure mode using the limit analysis of plasticity. Although several studies have been conducted to investigate the behavior of footings on stabilized sandy slopes (Huang et al., 1994; Yoo, 2001; Alawaji, 2001; El Sawwaf, 2005), the performance of a footing on a GRS abutment wall has not yet been well investigated and understood. Prior to development of a design method for this application, it is necessary to understand the behavior of the GRS abutment wall under static loading of different magnitude and offset distance to the wall facing. Geosynthetics can be connected to wall facing by the friction between the geosynthetic and blocks or a mechanical connector. Nicks et al. (2013) demonstrated that the wall facing had an apparent effect on the load-carrying capacity of the footing on the GRS pier. In other words, the geosynthetic-facing connection has an effect on the performance of the GRS pier. Wu and Pham (2013) treated closely-spaced geosynthetic-reinforced soil mass as a composite and developed a solution to calculate the load-carrying capacity of the GRS mass. This solution is suitable for isolated GRS piers under uniform axial loads, but may not be appropriate for GRS walls with retained soil under localized loads.

The main objectives of this study are to evaluate the relationship between the ultimate bearing capacity of the strip footing and the offset distance of the strip footing to the wall facing, identify possible failure modes of the wall, and investigate the effect of the mode of connection between geosynthetic and wall facing. To achieve these objectives, model GRS walls with a reduced size by a factor of 1/5 to a typical field scale were constructed and tested under strip footing loads in the laboratory. This study investigated the following influence factors: the offset distance of the footing, the length of geogrid reinforcement, the connection mode between geogrid and facing blocks, and the width of the footing.

The composite behavior of GRS walls is important for a system with close reinforcement spacing under a working load when it is used to support bridge footings to meet the serviceability requirement. Our study, however, is focused on the ultimate bearing capacity and stability (i.e., limit states) of the GRS wall. Under such conditions, the composite behavior is not that important. To achieve the limit states, the strengths of the fill and the geogrid have to be reduced. This method, so-called the strength reduction method, has been commonly used for theoretical development and model tests and was adopted in this study by using reduced-strength backfill and geogrid. More importantly, our model test results were verified by the limit equilibrium method.

2. Model tests

2.1. Test apparatus

A series of reduced-scale model tests were conducted to investigate the behavior of the GRS walls on rigid foundations subjected to static loading at different offset distances to the wall facing. The sizes of model walls were designed at a scale ratio of 1/5 to those of typical field walls. The main components of the experimental apparatus included a loading frame with a platform, an air cylinder, a test box, loading plates, and dial gauges. The box with inside dimensions of 1.5 m (length) × 0.4 m (width) × 0.8 m (height), was made of wood in three sides. The front side of the box was made of 20 mm thick toughened glass and was placed directly on the platform, as shown in Fig. 2. The glass wall allowed the observation and photogrammetry of the failure modes and deformations of the GRS walls during construction and loading. To minimize the side effect due to the friction of the wooden side wall of the box, a 1.5 mm thick transparent plastic sheet was fixed on the inside of the wooden side wall. Tognon et al. (1999) showed that polyethylene plastic sheets were placed on the walls of the box to minimize the angle of friction between the walls and soil to less than 5°. At the same time, a pair of jacks were placed on the outer faces of the box to ensure the rigidity of the box. The loading system

Please cite this article in press as: Xiao, C., et al., Experimental study on performance of geosynthetic-reinforced soil model walls on rigid foundations subjected to static footing loading, Geotextiles and Geomembranes (2015), http://dx.doi.org/10.1016/j.geotexmem.2015.06.001

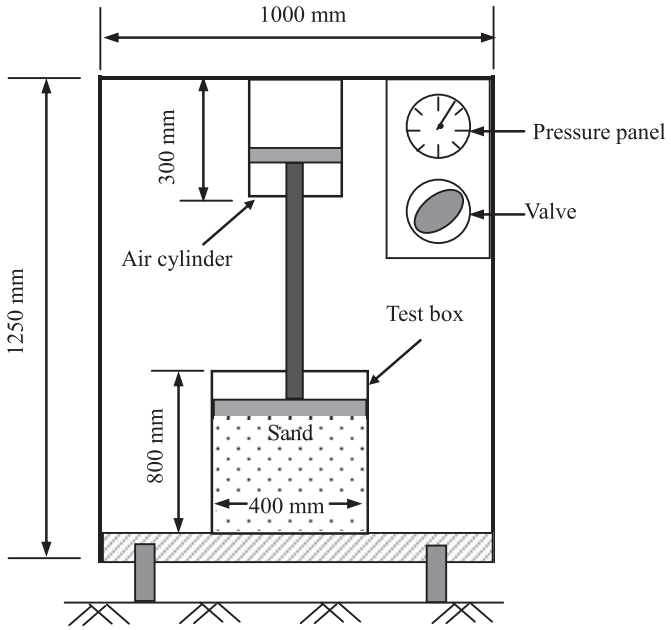

Fig. 2. Schematic diagram of the test apparatus.

consisted of an air cylinder, which was controlled by a hand-operated valve and a pressure panel to apply a load. Fig. 3 presents the test setup of a model wall.

2.2. Strip footing

Two steel plates of different widths were used to simulate strip footings. Both plates were 395 mm in length and 25 mm in thickness, but had the widths of 120 and 150 mm, respectively, which correspond to field footing sizes of 600 and 750 mm. To obtain the plane strain condition, the length of the plates was almost equal to the width of the test box.

2.3. Backfill soil

A pooly-graded dry river sand was used in the model tests. This sand was selected to simulate a reduced-size and strength backfill.

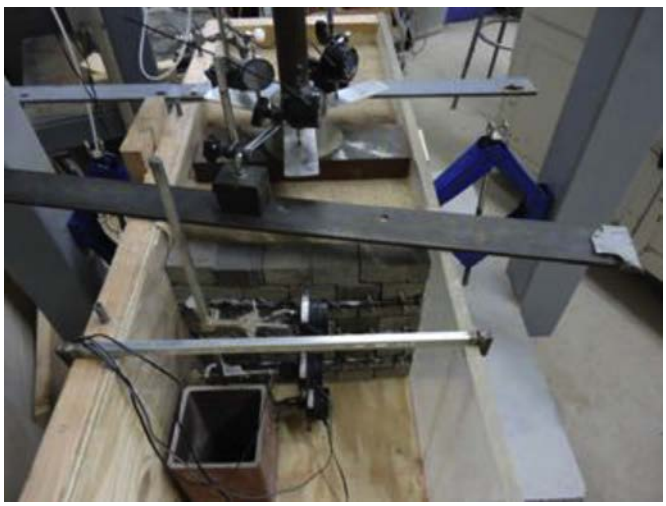

Fig. 3. Test setup of a test wall.

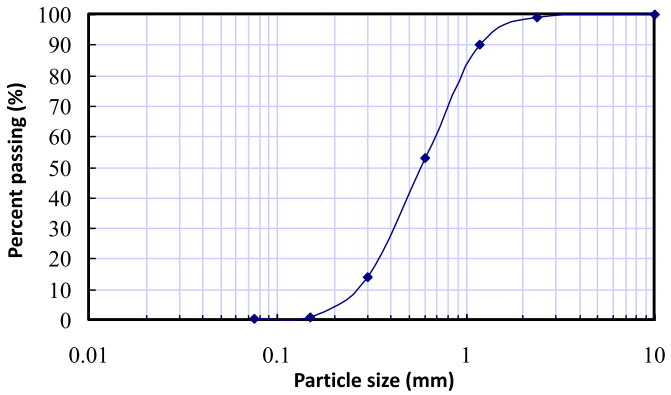

Fig. 4. Grain size distribution of the sand.

The sieve analysis tests were conducted following ASTM D422-63 and the grain size distribution curve of the sand is shown in Fig. 4. The mean grain size (D_{50}) was 0.55 mm and the uniformity coefficient (C_u) and the coefficient of curvature (C_c) of the sand were 2.53 and 0.93, respectively. The maximum and minimum dry unit weights of the sand were γ_{max} = 18.75 kN/m^3 and γ_{min} = 16.29 kN/m^3, respectively. The density of the backfill was achieved by compaction with fixed mass of sand into a pre-calculated volume of each lift. The target relative density of the backfill was 70%. The peak friction angle of the sand at 70% relative density was 40° based on the triaxial tests.

2.4. Properties of geogrid

Punched-drawn biaxial geogrid made of polypropylene material was used in the model tests. The geogrid had ultimate tensile strengths of 12.4 kN/m in the machine direction and 19 kN/m in the cross-machine direction based on the manufacturer's data. The properties of the biaxial geogrid obtained from the manufacturer are given in Table 1. Considering the fact that uniaxial geogrids are more commonly used in GRS walls (Abu-Hejleh et al., 2000, 2001; Pierson et al., 2011), two ribs of a biaxial geogrid in the machine direction were removed every four ribs to create a configuration of uniaxial geogrid in this study. Punched-drawn uniaxial geogrids typically have the aperture size in the longitudinal direction of 300–500 mm. Considering a scale ratio of 1/5, the aperture of the model geogrid in the longitudinal direction should be 60–100 mm. The model geogrid used in this study had the aperture length of 99 mm, which is within this range. Different from roadway applications, the geogrid in the GRS wall is mainly used to provide tensile strength. The aperture size is not that important, except for the pullout capacity. However, when the reinforcement length is 0.7 times the wall height or longer, pullout is often not an issue.

To keep the balance of facing units, the front-end transverse ribs of the geogrid to be connected with the facing units were not cut off, as shown in Fig. 5. To determine the tensile strength of the geogrid in the cross-machine direction after the removal of some

Table 1
Properties of the geogrid (provided by the manufacturer).

Index properties	MD	XMD
Aperture dimensions (mm)	25	33
Minimum rib thickness (mm)	0.76	0.76
Tensile strength at 2% strain (kN/m)	4.1	6.6
Tensile strength at 5% strain (kN/m)	8.5	13.4
Ultimate tensile strength (kN/m)	12.4	19.0

Note: MD stands for machine direction; XMD stands for cross-machine direction.

Please cite this article in press as: Xiao, C., et al., Experimental study on performance of geosynthetic-reinforced soil model walls on rigid foundations subjected to static footing loading, Geotextiles and Geomembranes (2015), http://dx.doi.org/10.1016/j.geotexmem.2015.06.001

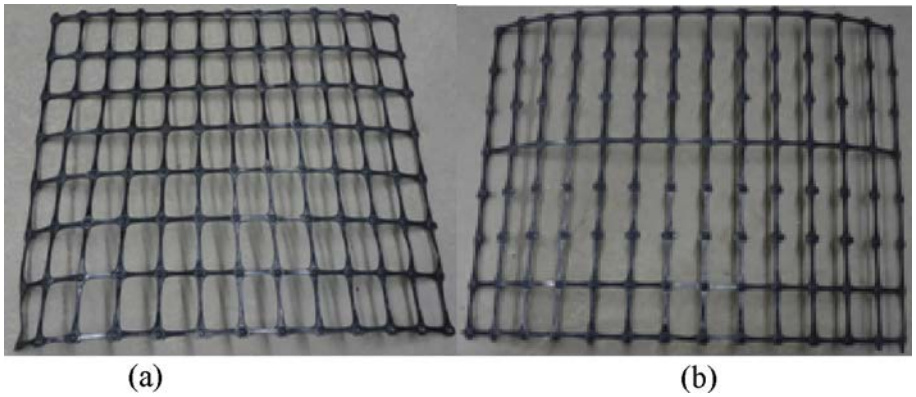

Fig. 5. Geogrid: (a) before ribs cut off, (b) after ribs cut off (used in the tests).

ribs, tensile tests with and without removed ribs were carried out following ASTM D6637. The test results in Fig. 6 show that the removal of partial ribs in the machine direction did not significantly influence the tensile strength of the geogrid in the cross-machine direction (i.e., 18.3 kN/m and 17.6 kN/m before and after the removal of partial ribs).

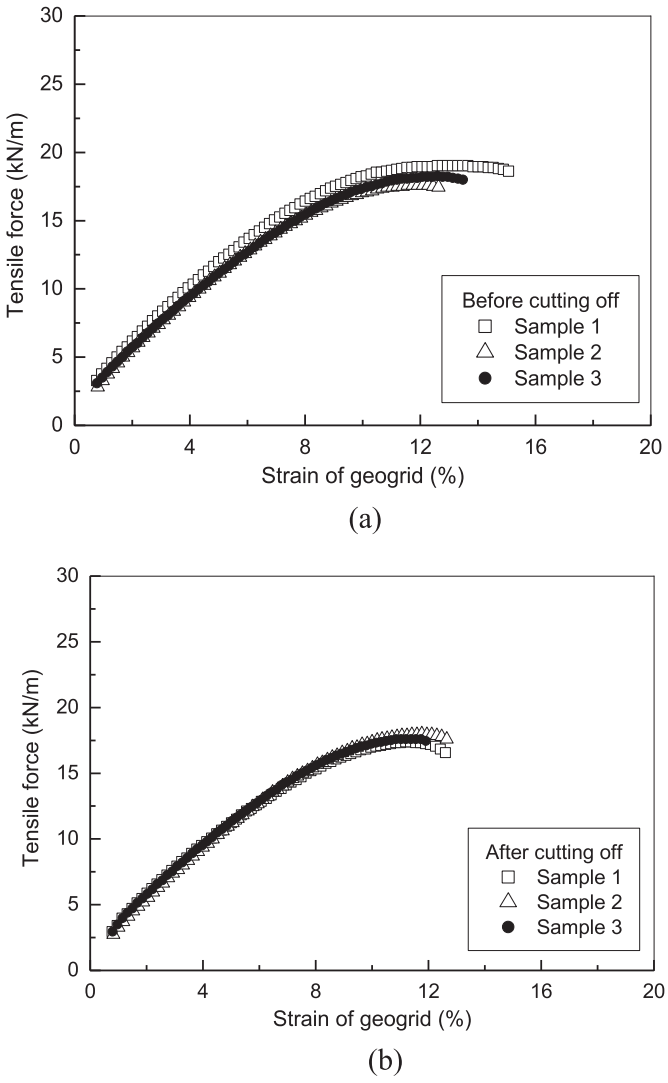

Fig. 6. Tensile strength tests of biaxial geogrid.

The typical tensile strengths of punched-drawn uniaxial geogrids range from 58 to 210 kN/m (Tensar International, 2012). The selection of the type of the biaxial geogrid for model tests was also based on the model scale effect. To simulate the possible internal failure of the wall under self-weight, the tensile strength of the model geogrid should be reduced to 1/25 that of a field geogrid because the total lateral earth force is proportional to H^2 (H is the wall height). However, if the internal failure is possibly induced by surcharge or footing pressure, the total lateral earth force is proportional to H. In this study, the failure of model walls was induced by the footing pressure; therefore, the tensile strength of the model geogrid should be reduced to 1/5 that of a field geogrid (i.e., 12–42 kN/m). The tensile strength of the model geogrid is within this range.

2.5. Facing blocks

Individual model wall facing units (blocks) with a dimension of 45 mm (height) × 50 mm (width) × 50 mm (length), were prepared by cutting plain concrete blocks as shown in Fig. 7. These blocks were used to simulate the facing blocks used in segmental

Fig. 7. Wall facing blocks.

Please cite this article in press as: Xiao, C., et al., Experimental study on performance of geosynthetic-reinforced soil model walls on rigid foundations subjected to static footing loading, Geotextiles and Geomembranes (2015), http://dx.doi.org/10.1016/j.geotexmem.2015.06.001

block walls. In the practice, there are a variety of block sizes used for GRS walls. The common one has a dimension of 200 mm (height), 250 mm (width), and 300 mm (length). Therefore, the ratio of the model block size to the field block size is approximately 1:5.

2.6. Connection modes between geogrid and blocks

In the practice, there are two typical connection modes between geogrid and blocks in GRS walls, i.e., mechanical and frictional connections. The importance of connection between geogrid and blocks has been widely recognized in the application of GRS walls. However, limited studies have been done to investigate the effect of the connection mode on the performance of GRS walls. In this study, two connection modes were modeled as shown in Fig. 8. The mechanical connection was created by inserting a steel bar through the aperture of the geogrid and fixing it with tapes between two adjacent blocks. Under such a condition, the geogrid would not be pulled out from the facing between the blocks. The frictional connection was modeled by inserting a piece of a geogrid rib into the front end of the geogrid layer without any fixture so that the geogrid could move between the blocks.

2.7. Test plan

GRS model wall tests were conducted to investigate the effects of the width of the loading plate (B_f), the ratio of the offset distance (D) to the height of wall (H), and the connection mode between geogrid and facing on the performance of GRS walls on rigid foundations under static strip loading. Fig. 9 shows the typical cross section of the model walls. All the model walls had the height of 360 mm and geogrid spacing (S) of 90 mm. The common geogrid spacing used in the field ranges from 200 to 600 mm. The scale ratio used to design the model walls in this study was 1/5. In other words, the model vertical spacing of 90 mm corresponds to the field vertical spacing of 450 mm, which is within the typical spacing range in the field. Fig. 10 shows the layouts of the model tests with 0.7H long geogrid and at a different offset distance of the footing to the wall facing. The Rankine failure plane is plotted as well. This information can help identify the relative location of the loading plate to the stable zone and the active zone. To investigate the effect of the reinforcement length, six model walls were constructed with longer reinforcement (i.e., $L = 2H$). Table 2 tabulates the test plan. This study completed totally 30 model tests. Two digital dial gauges were placed on the footing to measure the settlement of the footing. Three digital dial gauges were placed at three elevations in front of the wall surface to measure the lateral deformations of the wall facing.

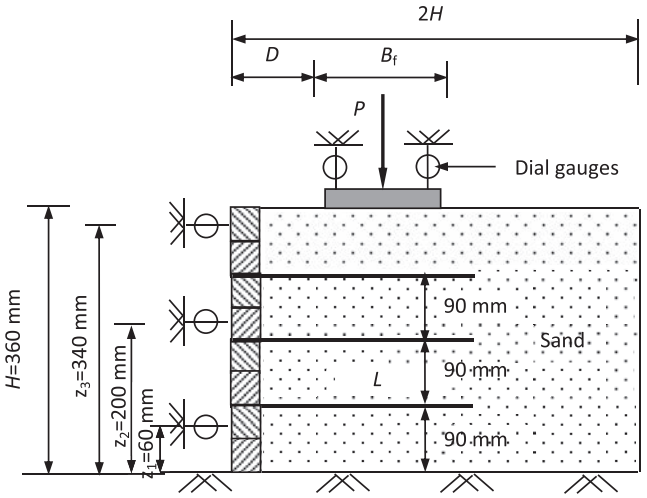

Fig. 9. Schematic view of model test.

3. Tests results and discussion

3.1. Time required for each loading increment

To determine the required time for each loading increment, a test was conducted with each loading increment of 25 kPa applied on the strip footing. The time required for each loading increment was determined based on the plate loading test with $B_f/H = 0.33$, $D/H = 0.4$, and frictional connection. In this test, each load after application was maintained for 30 min, during which the lateral displacements of the wall facing and the settlements of the loading plate were recorded every 5 min as shown in Fig. 11. Lateral displacements and settlements occurred immediately after the application of each load and continued increasing at a slow rate up to 10 min. After 10 min, further increases of the lateral displacement and the settlement were small and could be ignored. Therefore, 10 min for each loading increment were selected and adopted for all the later tests.

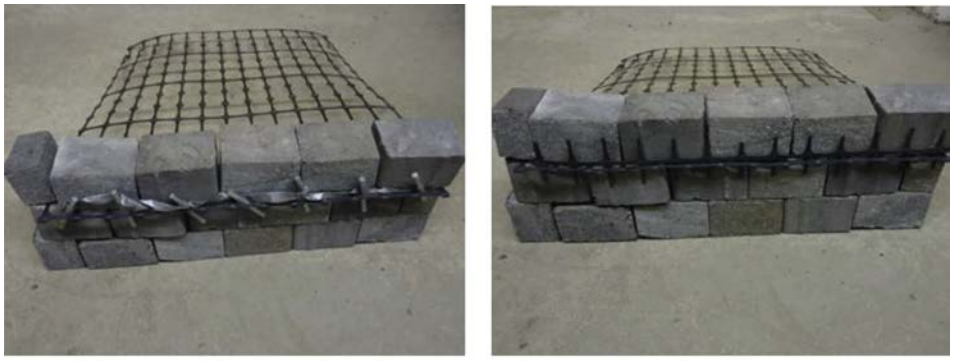

(a) (b)

Fig. 8. Connection modes between geogrid and blocks: (a) mechanical connection; (b) frictional connection.

Please cite this article in press as: Xiao, C., et al., Experimental study on performance of geosynthetic-reinforced soil model walls on rigid foundations subjected to static footing loading, Geotextiles and Geomembranes (2015), http://dx.doi.org/10.1016/j.geotexmem.2015.06.001

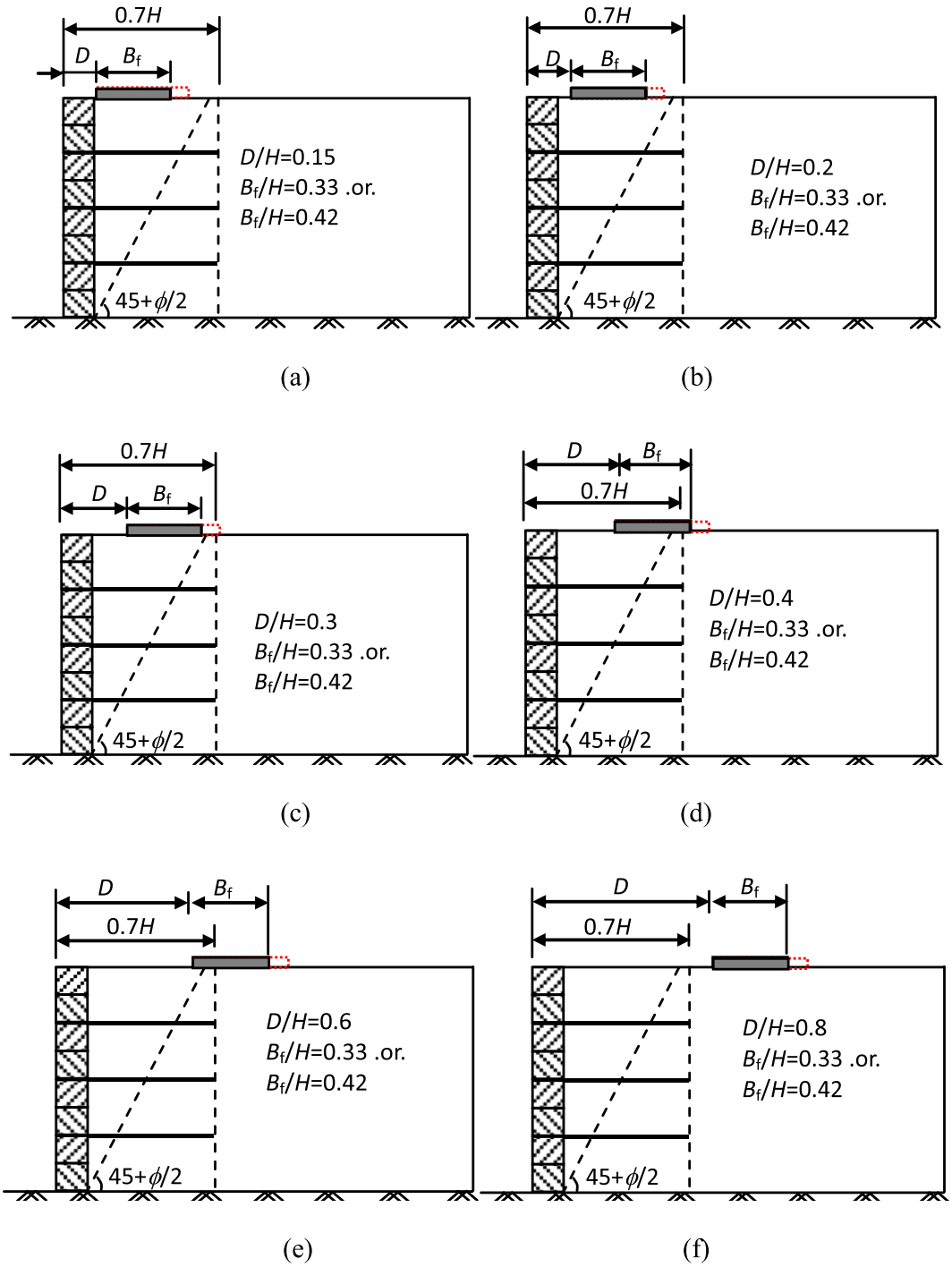

Fig. 10. Layout of the model tests with 0.7*H* long geogrid.

Please cite this article in press as: Xiao, C., et al., Experimental study on performance of geosynthetic-reinforced soil model walls on rigid foundations subjected to static footing loading, Geotextiles and Geomembranes (2015), http://dx.doi.org/10.1016/j.geotexmem.2015.06.001

Table 2
Model test plans.

Test amount	D/H	L/H	Connection mode	B_f (mm)	B_f/H
24	0.15, 0.2, 0.3, 0.4, 0.6, 0.8	0.7 or 2	Mechanical	120 or 150	0.33 or 0.42
6	0.15, 0.2, 0.3, 0.4, 0.6, 0.8	0.7	Frictional	120	0.33

3.2. Pressure-settlement curves of footings

The average settlement of the footing at each applied pressure was calculated based on the measurements by the two digital dial gauges. Since two footing sizes were used, for normalization, a ratio of settlement to footing width, s/B_f, is employed against the applied pressure as shown in Fig. 12. All the curves contain a nearly linear portion and a suddenly increased settlement portion under the last load. The failure of a test was defined as the state when the footing seated on the top surface of the wall could not carry any further load. The ultimate bearing capacity of the footing on the GRS walls was defined as the pressure before the last failure pressure in the test. Fig. 12 shows that the ultimate bearing capacity of the footing on the GRS wall depended on the offset distance of the footing, the length of the reinforcement, and the connection mode between geogrid and facing blocks.

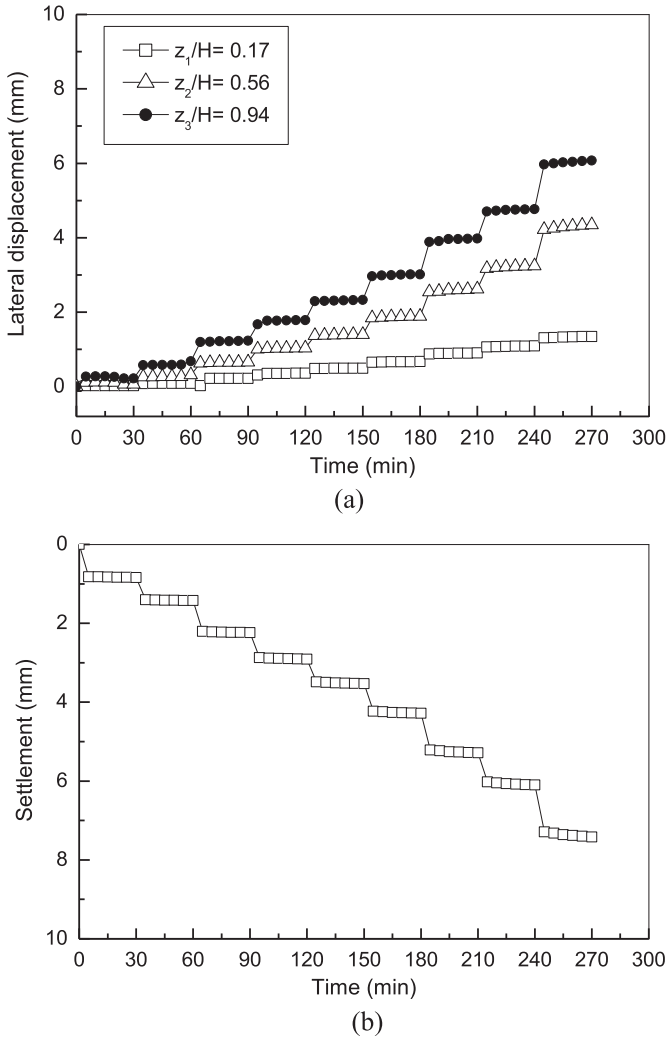

Fig. 11. Measured deformations of the GRS wall test: (a) lateral displacement of wall facing; (b) settlement of strip footing.

3.3. Effect of offset and width of strip footing

Fig. 13 shows the effect of the offset distance of the footing, D, on the ultimate bearing capacity of the footing on the GRS wall. In these tests, the mechanical connection between geogrid and blocks was used. Two sizes (i.e., $B_f/H = 0.33$ and 0.42) of strip footings were included. Fig. 13 shows that two sizes of footings resulted in a similar trend of the ultimate bearing capacity varying with the offset distance of the footing. With an increase of the D/H ratio, the ultimate bearing capacity increased and reached the maximum value at $D/H = 0.3$. When $D/H > 0.3$, the ultimate bearing capacity decreased with an increase of the D/H ratio until reaching a constant value at $D/H = 0.6$. Fig. 10 shows that the footing was almost out of the reinforced zone when $D/H = 0.6$. In other words, the ultimate bearing capacity was controlled by the unreinforced sand. Therefore, a further increase of the D/H ratio did not change the ultimate bearing capacity. In addition, Fig. 13 shows that the footing with the width of 150 mm resulted in a higher ultimate bearing capacity than the footing with the width of 120 mm and their difference became smaller when the D/H ratio increased.

3.4. Effect of reinforcement length

Fig. 14 shows the comparison of the test results at the geogrid length of $2H$ with those at the geogrid length of $0.7H$ and the variation of the ultimate bearing capacities with the offset distance of the footing in the tests at different geogrid length. The test results indicated that there was no obvious difference in the ultimate bearing capacity due to the geogrid length at the same B_f/H ratio when $D/H \leq 0.2$ (i.e., close to the wall facing). However, when $D/H > 0.2$ and $D/H < 0.4$, the difference in the ultimate bearing capacity became obvious and more significant with an increase of the D/H ratio. The ultimate bearing capacity became constant after $D/H > 0.4$ for the tests with $2H$ long reinforcements. This result can be explained by the fact that the offset distance of the footing to the wall facing was far enough so that the wall facing did not have any effect and the bearing capacity of the footing on the GRS wall was the same as the bearing capacity of the footing on the geogrid-reinforced soil with a flat ground. This result is consistent with those obtained by Yoo (2001) and El Sawwaf (2007), in which the bearing capacity of a footing on the reinforced slope remained constant when the offset distance of the footing was greater than $1.5B_f$ away from the slope crest.

3.5. Effect of connection mode

This study evaluated two connection modes (i.e., mechanical and frictional connections). Fig. 15 illustrates the effect of the connection mode on the ultimate bearing capacity of the footing. When the footing was close to the wall facing (i.e., $D/H < 0.4$), the tests with the mechanical connection yielded higher ultimate bearing capacities than those with the frictional connection. The influence of the connection mode became insignificant when $D/H \geq 0.4$ because the wall facing had an insignificant effect.

Please cite this article in press as: Xiao, C., et al., Experimental study on performance of geosynthetic-reinforced soil model walls on rigid foundations subjected to static footing loading, Geotextiles and Geomembranes (2015), http://dx.doi.org/10.1016/j.geotexmem.2015.06.001

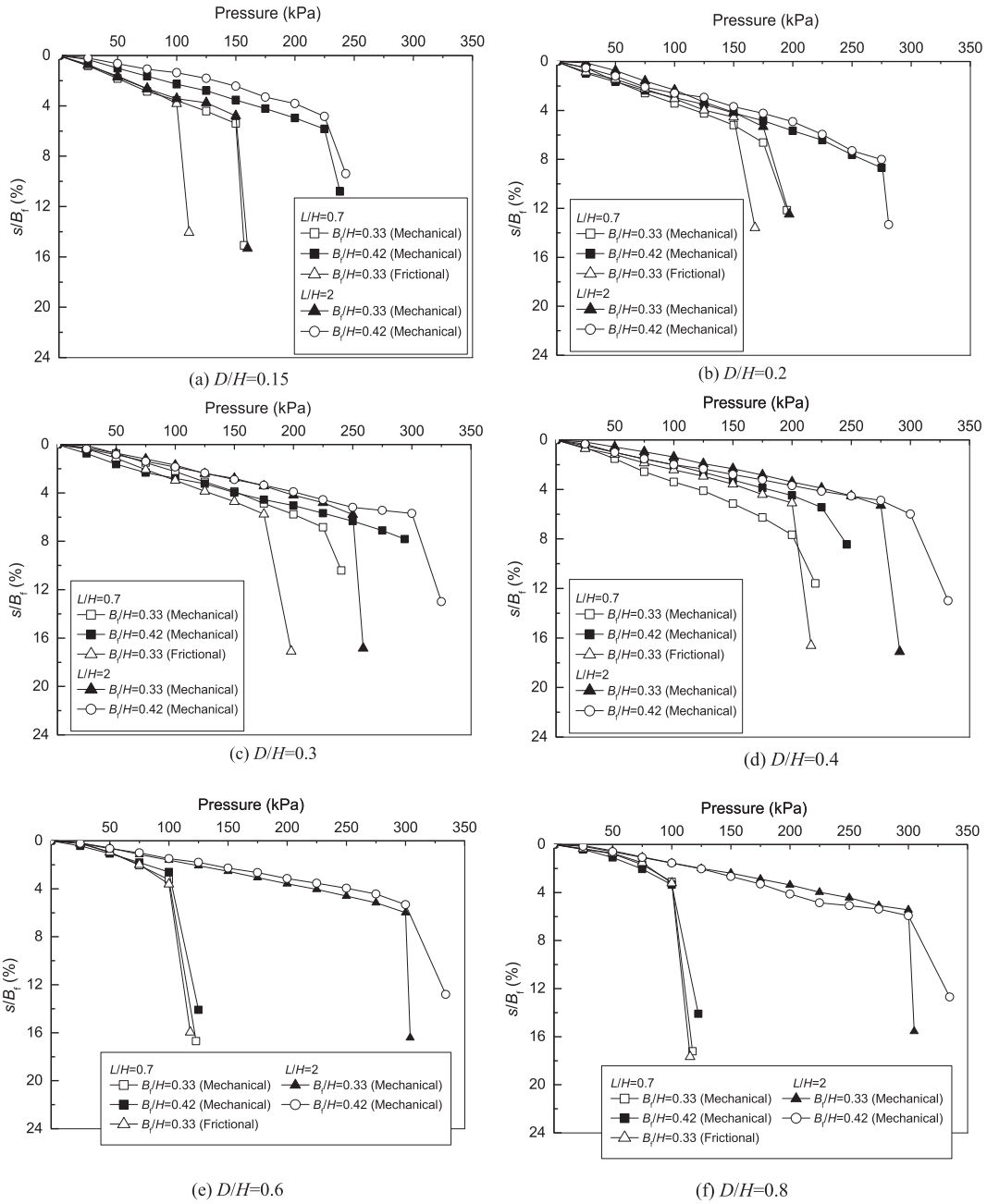

Fig. 12. Pressure-settlement curves of footings.

Please cite this article in press as: Xiao, C., et al., Experimental study on performance of geosynthetic-reinforced soil model walls on rigid foundations subjected to static footing loading, Geotextiles and Geomembranes (2015), http://dx.doi.org/10.1016/j.geotexmem.2015.06.001

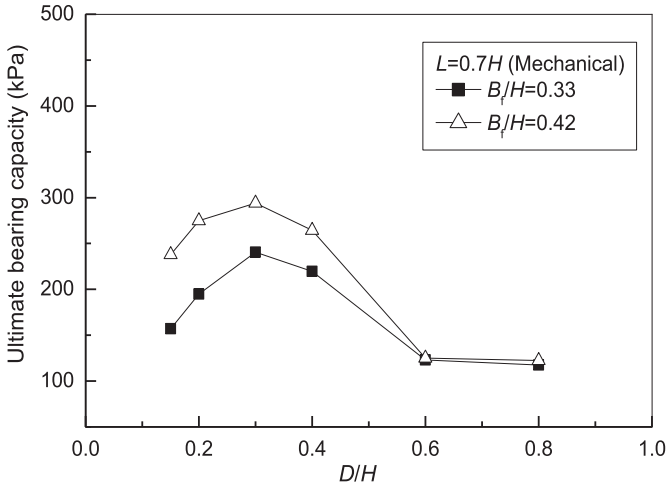

Fig. 13. Variation of bearing capacities of the footing on the GRS walls with D/H.

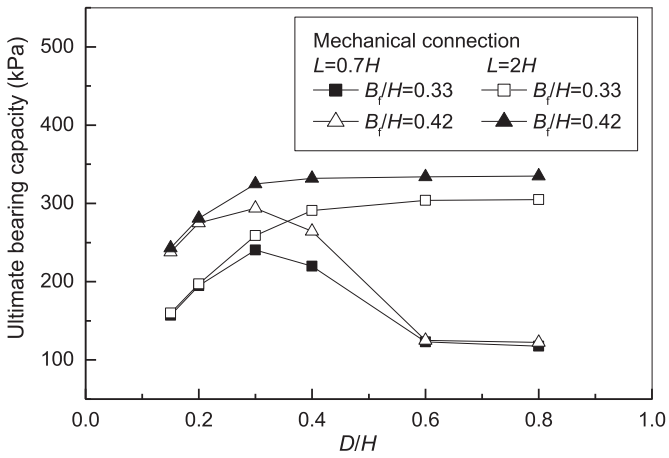

Fig. 14. Effect of reinforcement length on bearing capacities of the footing on GRS walls.

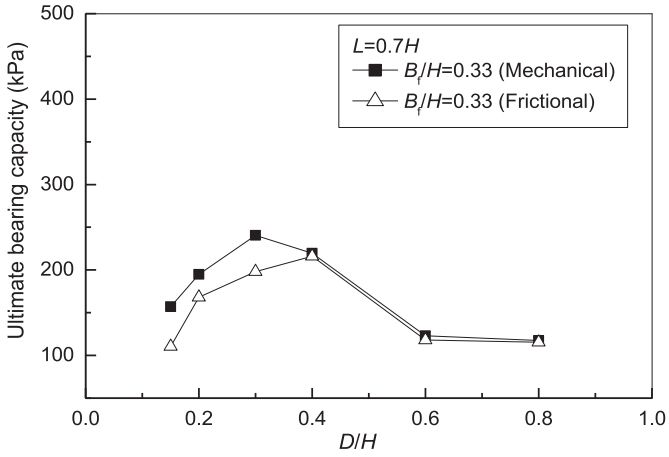

Fig. 15. Effect of connection mode on ultimate bearing capacities of the footing on the GRS walls.

3.6. Lateral deformation of wall facing

Three digital dial gauges were installed against the wall facing at three elevations to measure the lateral deformations of the wall facing under loading. Figs. 16 and 17 show that the lateral deformations of the wall facing of the GRS walls under the 120 mm wide footing. Apparently, the ratios of the lateral deformation to the height of the wall, d/H, were generally smaller than 2% before the failure of the GRS walls. The tests with the mechanical connection mode and/or with long reinforcement (i.e., $L = 2H$) reduced the lateral deformations of the wall facing as compared with the tests with the frictional connection and/or short reinforcement (i.e., $L = 0.7H$). Therefore, an increase of the reinforcement length and the connection strength between reinforcement and facing units are the feasible and effective approaches to reduce the lateral deformations of the GRS abutment walls.

Figs. 16 and 17 also show that the offset distance of the footing influenced the shape and magnitude of the lateral deformation of the wall facing. Before the failure pressure, the maximum lateral deformation of the wall facing occurred within the upper portion of the wall. Under the failure pressure, however, the maximum lateral deformation was still within the upper portion of the wall when $D/H \leq 0.4$ and the mechanical connection was used, while the maximum lateral deformation was in the middle of the wall facing in the test when $D/H > 0.4$ and the mechanical connection was used and all the tests when the frictional connection was used. Furthermore, at the same applied pressure, the lateral deformation decreased with an increase of the offset distance from the footing to the wall facing.

3.7. Analysis of failure modes of GRS walls

The 20 mm thick glass placed in the front side of the test box allowed the observation and photogrametry to study the deformation and failure mechanism of the GRS walls under loading. The images of the failed GRS walls with the $0.7H$ long reinforcement and the mechanical and frictional connections were used to evaluate the possible failure modes of the GRS walls under loading. To assist this evaluation, the limit equilibrium program, ReSSA version 3.0, developed by the ADAMA Engineering, Inc., was used to calculate the factors of safety and determine the critical slip surfaces using Bishop's modified method and Spencer's two-part wedge method. The peak friction angle of the backfill sand was 40° obtained from the triaxial tests. Considering the tests were conducted under the plane strain condition, the friction angle used in the limit equilibrium analysis was corrected to 44°, which is 1.1 times the friction angle from the triaxial tests (Kulhawy and Mayne, 1990). The interface friction angle between blocks was determined as 33° degree using the simple tilt table test, as shown in Fig. 18. Since the geogrid was connected to the blocks by the mechanical and frictional modes, there should be certain cohesion between blocks. The mechanical connection was stronger than the frictional connection. To calibrate the cohesion of the interface due to the connection modes, the cohesion value of the blocks was changed in the software until the computed factors of safety using Spencer's method for the two randomly selected cases (one with the mechanical connection and another with the frictional connection) at $D/H = 0.15$ approached to 1.0 under its corresponding ultimate bearing capacities. The cohesion values of the interface were determined as 75 kPa and 55 kPa in the cases with the mechanical and frictional connection, respectively and these values were used for all other tests. In all the limit equilibrium analyses, Spencer's method always resulted in a lower factor of safety than Bishop's method; therefore, Spencer's method was used for the cohesion calibration. The properties of the foundation were selected to ensure no slip surface

Please cite this article in press as: Xiao, C., et al., Experimental study on performance of geosynthetic-reinforced soil model walls on rigid foundations subjected to static footing loading, Geotextiles and Geomembranes (2015), http://dx.doi.org/10.1016/j.geotexmem.2015.06.001

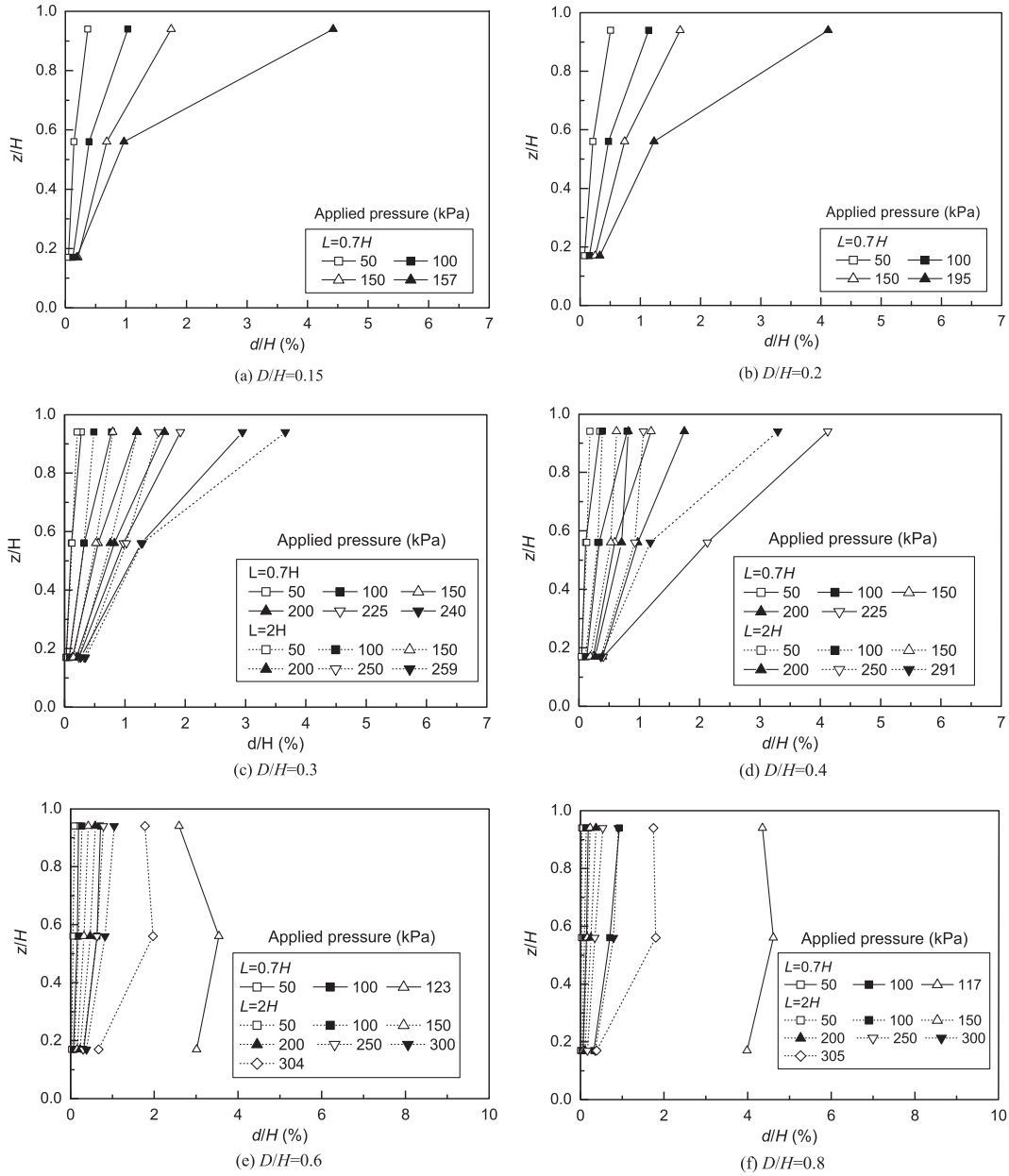

Fig. 16. Lateral deformations of the wall facing at different reinforcement lengths and D/H ratios when the mechanical connection was used.

occurring within the foundation. Table 3 shows the material properties used in the limit equilibrium analysis.

Fig. 19 shows the slip surfaces in the test walls with the mechanical connection at failure. The observed slip surfaces were plotted using the dot lines. These slip surfaces were traced based on the distortions of the colored sand layers and the wall facing. The slip surfaces in solid lines and their corresponding factors of safety using the limit equilibrium analysis were plotted as well. The bilinear solid line was from Spencer's method while the circular line was from Bishop's method. Based on the observations, the slip surfaces started from the one-side edge of the footing and developed through the geogrid layers toward the wall facing. It is a general observation that three slip surfaces developed in the backfill: a shallow one, a middle one, and a deep one. The wall failed through one of the slip surfaces. When the footing was close to the wall facing (i.e., $D/H = 0.15$, 0.2, and 0.3), the blocks within the upper portion had obvious relative movement. When the footing was far away from the wall facing, the wall facing titled outward entirely. The factors of safety calculated by Spencer's two-part wedge method were close to 1 for all the cases and were smaller than those by Bishop's method. This comparison indicates that the two-part wedge failure was more critical than the circular failure. The critical slip surface identified by Spencer's two-part wedge method agreed well with one of the observed slip surfaces in all the cases.

Fig. 20 shows the slip surfaces in the test walls with the frictional connection at failure. Also, the slip surfaces by observation and the limit equilibrium analysis were included. The slip surface started from the one-side edge of the footing as well. Different from the test walls with the mechanical connection, however, there was obvious relative movement between blocks in all tests due to the weak connection between geogrid and facing blocks. In addition, the walls with the frictional connection had shallower slip surfaces

Please cite this article in press as: Xiao, C., et al., Experimental study on performance of geosynthetic-reinforced soil model walls on rigid foundations subjected to static footing loading, Geotextiles and Geomembranes (2015), http://dx.doi.org/10.1016/j.geotexmem.2015.06.001

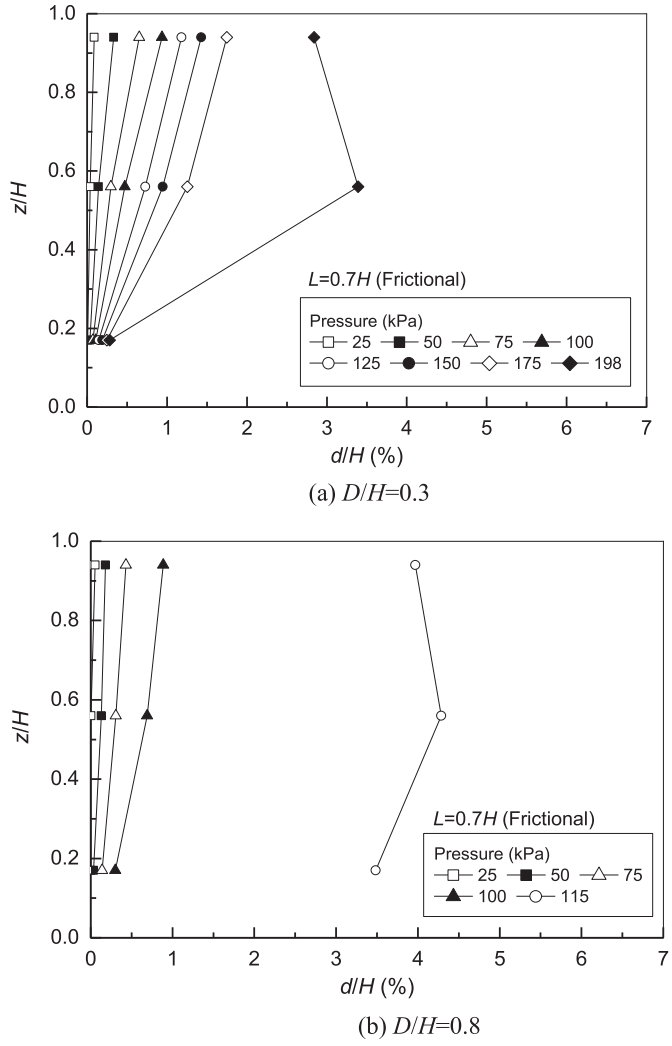

Fig. 17. Lateral deformations of the wall facing with 0.7*H* long reinforcement when the frictional connection was used.

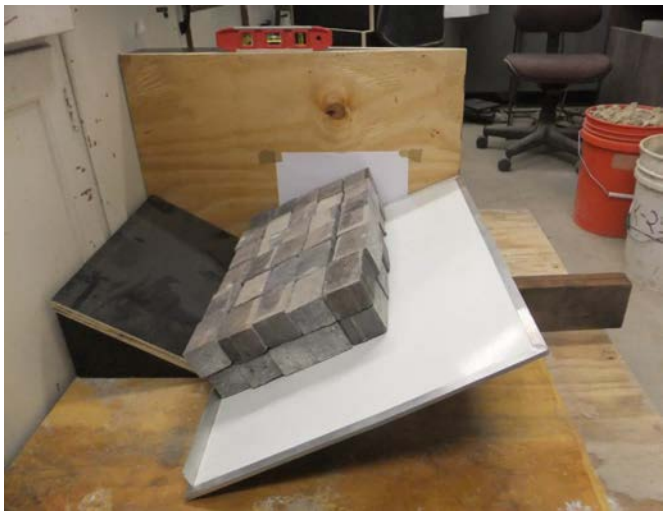

Fig. 18. Setup of the tilt table test.

Table 3
Material properties.

Material	Properties
Backfill	$\gamma = 17.9$ kN/m^3, $\varphi = 44^\circ$, $c = 0$
Blocks	$\gamma = 20$ kN/m^3, $\varphi = 33^\circ$, $c = 75/55$ kPa
Foundation	$\gamma = 20$ kN/m^3, $\varphi = 35^\circ$, $c = 200$ kPa
Geogrid	$T_u = 19$ kN/m, $T_c = T_u$, $c_i = 0.8$

Note: T_u = tensile strength of geogrid; T_c = connection strength of geogrid; c_i = interaction coefficient between geogrid and backfill.

than those with the mechanical connection. This comparison indicated that the walls with the frictional connection were more flexible than those with the mechanical connection. The results of the limit equilibrium analysis show that the factors of safety by Spencer's method were lower than those by Bishop's method. The critical slip surface identified by Spencer's method had a good agreement with one of the observed slip surfaces.

4. Conclusions

This paper presents 30 instrumented model tests to investigate the performance of the GRS walls on rigid foundations subjected to static strip loading. Four influence factors were considered: (1) offset distance of footing (D), (2) width of footing (B_f), (3) length of reinforcement (L), and (4) connection mode between geogrid and blocks. Based on the test results, the following conclusions can be drawn:

(1) When the GRS walls had the reinforcement length of 0.7*H* (*H* is the wall height), the maximum ultimate bearing capacity occurred at $D/H = 0.3$ with the mechanical connection or $D/H = 0.4$ with the frictional connection. This maximum ultimate bearing capacity existed because of the transition between the reinforced and unreinforced zone. However, the ultimate bearing capacity decreased to a constant value at $D/H = 0.6$ with an increase in the offset distance of the footing from the back of the wall. This constant value was controlled by the strength of the unreinforced sand. When the GRS walls had the longer reinforcement length (2*H*), however, the ultimate bearing capacity increased with the D/H ratio and became constant when D/H was greater than 0.4. This constant value was controlled by the strength of the reinforced sand. The use of the mechanical connection increased the maximum ultimate bearing capacity of the footing by 10% as compared with the frictional connection.

(2) The ratios of the lateral deformation of the wall facing to the height of the wall were generally smaller than 2% with the reinforcement length of $L = 0.7H$ and smaller than 1% with the reinforcement length of $L = 2H$ before the failure of the GRS walls. The offset distance of the footing influenced the shape of the lateral deformation of the wall facing. At the failure pressure, the maximum lateral displacement was within the upper portion of the wall when $D/H \leq 0.4$ and the mechanical connection was used, while the maximum lateral deformation was in the middle portion of the wall facing in the tests when $D/H > 0.4$ and the mechanical connection was used and all the tests when the frictional connection was used.

(3) It is a general observation that the failure surface started from the one-side edge of the footing. Three potential slip surfaces were observed from the tests with the mechanical connection, exiting from the wall facing at shallow, middle, and deep depths. The slip surfaces in the walls with the frictional connection tended to happen at shallower depths

Please cite this article in press as: Xiao, C., et al., Experimental study on performance of geosynthetic-reinforced soil model walls on rigid foundations subjected to static footing loading, Geotextiles and Geomembranes (2015), http://dx.doi.org/10.1016/j.geotexmem.2015.06.001

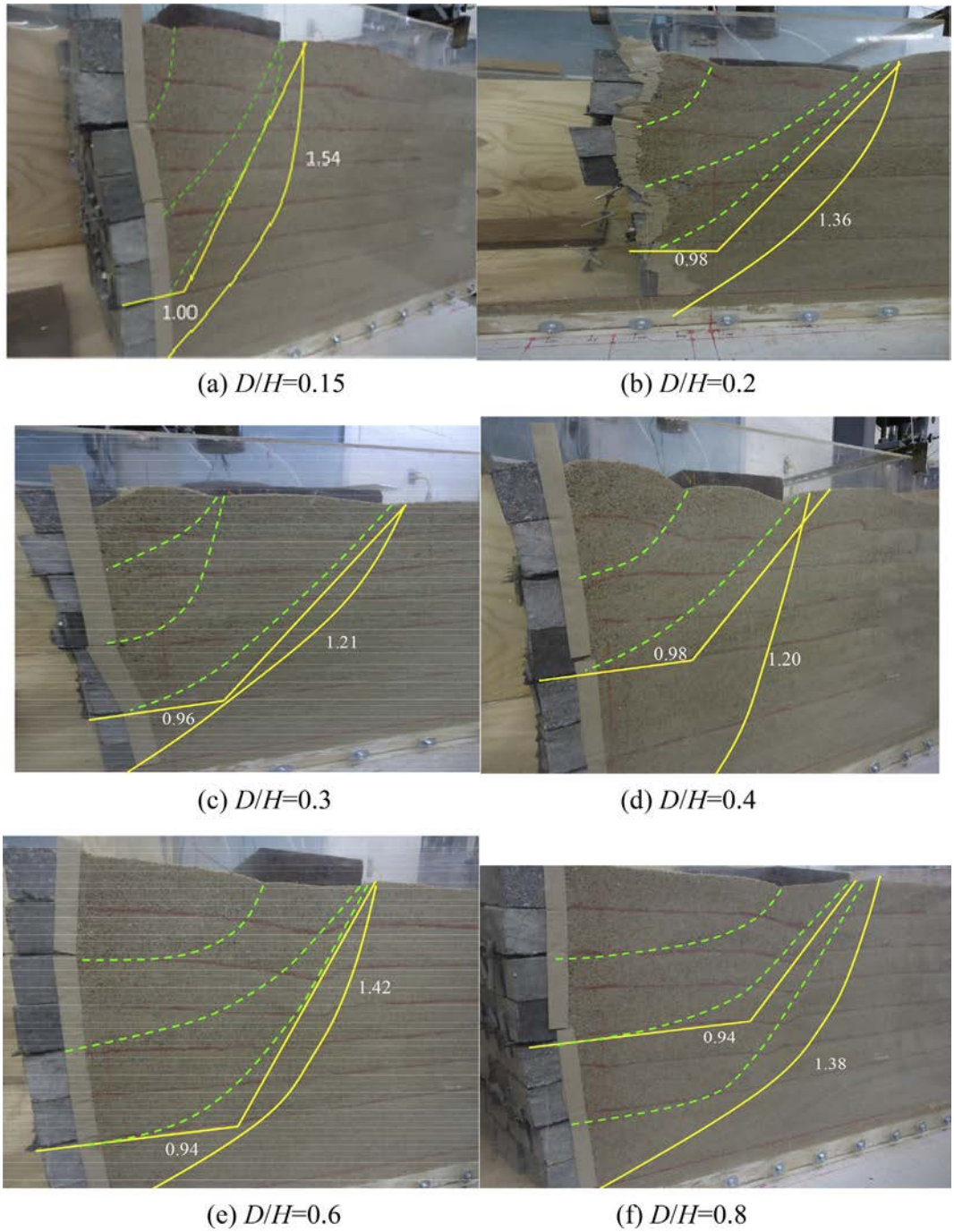

Fig. 19. Failure modes of the test walls with the mechanical connection.

Please cite this article in press as: Xiao, C., et al., Experimental study on performance of geosynthetic-reinforced soil model walls on rigid foundations subjected to static footing loading, Geotextiles and Geomembranes (2015), http://dx.doi.org/10.1016/j.geotexmem.2015.06.001

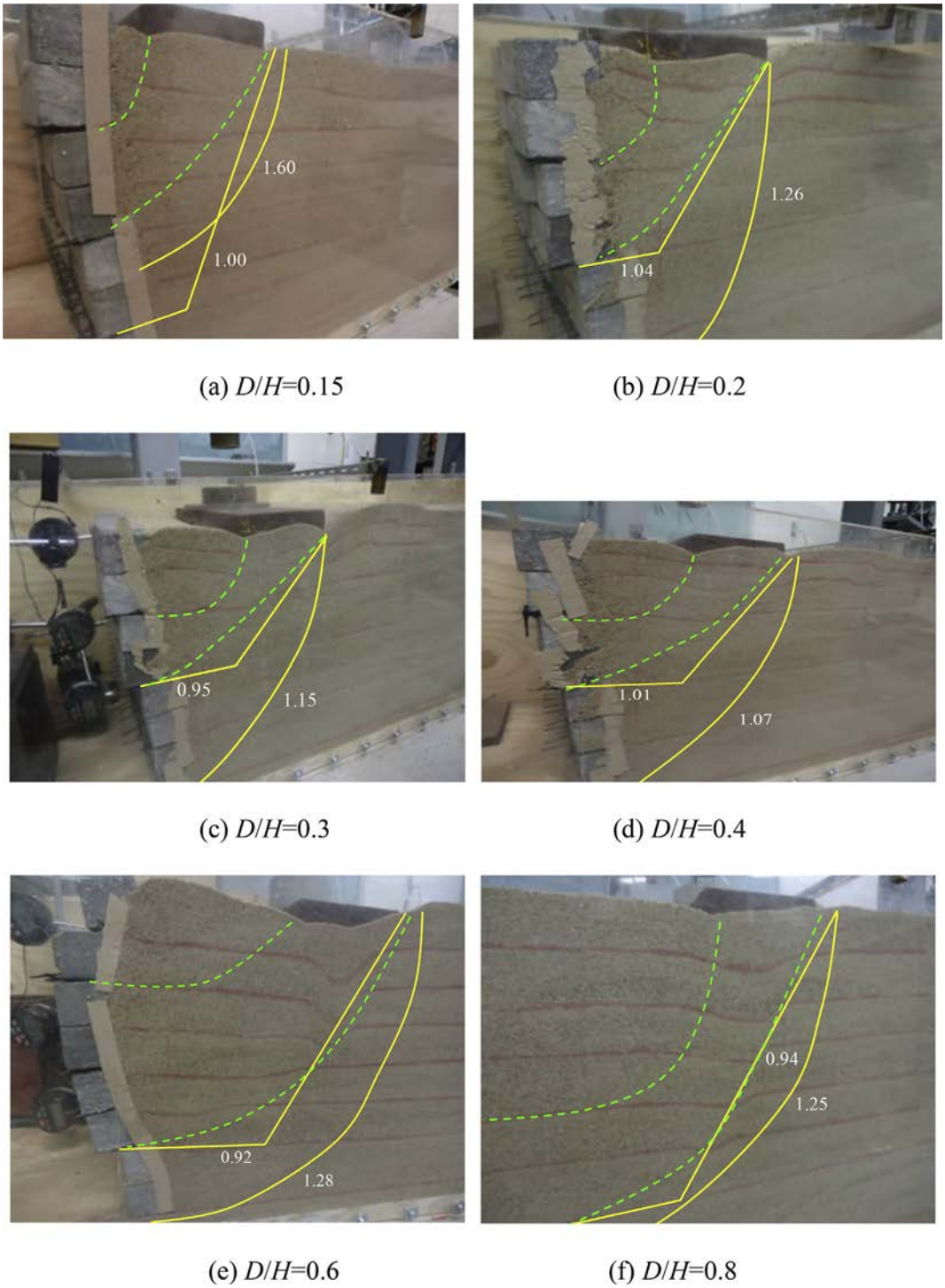

Fig. 20. Failure modes of the test walls with the frictional connection.

Please cite this article in press as: Xiao, C., et al., Experimental study on performance of geosynthetic-reinforced soil model walls on rigid foundations subjected to static footing loading, Geotextiles and Geomembranes (2015), http://dx.doi.org/10.1016/j.geotexmem.2015.06.001

than those with the mechanical connection. The limit equilibrium analyses show that Spencer's two-part wedge method resulted in lower factors of safety than Bishop's circular slip surface method. Spencer's method identified the critical slip surfaces with factors of safety close to 1.0, which reasonably matched one of the slip surfaces observed in the tests.

Acknowledgment

This research work was conducted when the first author visited the University of Kansas as a visiting scholar, which was sponsored by the China Scholarship Council, and extended when the third author visited the University of Kansas as a visiting student, which was partially sponsored by the scholarship of short-term abroad visiting for a Ph.D candidate in Tongji University, China. This research work was also supported by Grant No. 50909032 and E2014202038 from the Natural Science Foundation of China and Hebei Province Natural Science Foundation. Their financial support is gratefully acknowledged.

References

Abu-Hejleh, N., Wang, T., Zornberg, J.G., 2000. Performance of geosynthetic-reinforced walls supporting bridge and approaching roadway structures. In: ASCE Geotechnical Special Publication No. 103. ASCE, Reston, VA, United States, pp. 218–243.

Abu-Hejleh, Zornberg, J.G., Wang, T., 2001. Performance of Geosynthetic-reinforced Walls Supporting the Founders/Meadows Bridge and Approaching Roadway Structures. Report from Colorado Department of Transportation Research Branch, Report No. CDOT-DTD-R-2001-12.

ADAMA Engineering, Inc, 2008. ReSSA Software Version 3.0 Newark, Delaware, USA.

Adams, M.T., 1997. Performance of prestrained geosynthetic reinforced soil bridge piers. In: Wu, J.T.H., Barrett, R. (Eds.), Mechanically Stabilized Backfill. A.A. Balkema Publisher, Rotterdam, pp. 35–53.

Adams, M.T., Collin, J.G., 1997. Large model spread footing load tests on geosynthetic reinforced soil foundation. J. Geotech. Geoenviron. Eng. 123 (1), 66–72.

Alawaji, H.A., 2001. Settlement and bearing capacity of geogrid-reinforced sand over collapsible soil. Geotext. Geomemb. 19 (2), 75–88.

ASTMD6637. Standard Test Method for Determining Tensile Properties of Geogrids by the Single or Multi-rib Tensile Method. American Society for Testing and Materials, West Conshohocken, Pennsylvania, USA.

ASTM D422-63. Standard Test Method for Particle-Size Analysis of Soils. American Society for Testing and Materials, West Conshohocken, Pennsylvania, USA.

Berg, R.R., Christopher, B.R., Samtani, N.C., 2009. Design and Construction of Mechanically Stabilized Earth Walls and Reinforced Soil Slopes. Publication No. FHWA-NHI-10-024. Federal Highway Administration.

Bilgin, Ö., 2009. Failure mechanisms governing reinforcement length of geogrid reinforced soil retaining walls. Eng. Struct. 31 (9), 1967–1975.

Bourgeois, E., Soyez, L., Le Kouby, A., 2011. Experimental and numerical study of the behavior of a reinforced earth wall subjected to a local load. Comput. Geotech. 38 (4), 515–525.

Elias, V., Christopher, B.R., Berg, R.R., 2001. Mechanically Stabilized Earth Walls and Reinforced Soil Slopes Design and Construction Guidelines. Publication No. FHWA-NHI-00–043. Federal Highway Administration.

El Sawwaf, M.A., 2005. Strip footing behavior on pile and sheet pile stabilized sand slope. J. Geotech. Geoenviron. Eng. 131 (6), 705–715.

El Sawwaf, M.A., 2007. Behavior of strip footing on geogrid-reinforced sand over a soft clay slope. Geotext. Geomemb. 25 (1), 50–60.

Han, J., Leshchinsky, D., 2010. Analysis of back-to-back mechanically stabilized earthwalls. Geotext. Geomemb. 28 (3), 262–267.

Hara, T., Yu, Y., Ugai, K., 2004. Behaviour of piled bridge abutments on soft ground: a design method proposal based on 2D elasto-plastic-consolidation coupled FEM. Comput. Geotech. 31 (4), 339–355.

Helwany, S.M.B., Wu, J.T.H., Froessl, B., 2003. GRS bridge abutments-an effective means to alleviate bridge approach settlement. Geotext. Geomemb. 21 (3), 177–196.

Huang, C.-C., Tatsuoka, F., Sato, Y., 1994. Failure mechanisms of reinforced sand slopes loaded with a footing. Soils Found. 34 (2), 27–40.

Huang, J., Parsons, R.L., Han, J., Pierson, M., 2011. Numerical analysis of a laterally loaded shaft constructed within an MSE wall. Geotext. Geomemb. 29 (3), 233–241.

Huang, J., Han, J., Parsons, R.L., Pierson, M., 2013. Refined numerical modeling of a laterally-loaded drilled shaft in an MSE wall. Geotext. Geomemb. 37, 61–73.

Huang, J., Bin-Shafique, S., Han, J., Rahman, M.S., 2014. Modeling of laterally loaded drilled shaft group in MSE wall. ICE Geotech. Eng. J. 167 (GE4), 402–414.

Ketchart, K., Wu, J.T.H., 1997. Performance of GRS bridge pier and abutment in Denver, CO, USA. In: Barrett, Wu (Ed.), Special Presentation, Mechanically Stabilized Backfill. A. A. Balkema Publisher, Rotterdam, pp. 101–116.

Koerner, R.M., 1996. Designing with Geosynthetics, fourth ed. Prentice-Hall Inc, New Jersey: Englewood Cliffs.

Kulhawy, F.H., Mayne, P.H., 1990. Manual on Estimating Soil Properties for Foundation Design. Report EL-6800 Electric Power Research Institute, EPRI, August.

Leshchinsky, B., 2014. Limit analysis optimization of design factors for mechanically stabilized earth wall-supported footings. Transp. Infrastruct. Geotech. 1, 111–128.

Leshchinsky, D., Han, J., 2004. Geosynthetic reinforced multitiered walls. ASCE J. Geotech. Geoenviron. Eng. 130 (12), 1225–1235.

Ling, H.I., Leshchinsky, D., Wang, J.-P., Mohri, Y., Rosen, A., 2009. Seismic response of geocell retaining walls: experimental studies. ASCE J. Geotech. Geoenviron. Eng. 135 (4), 515–524.

Nicks, J.E., Adams, M.T., Ooi, P.S.K., Stabile, T., 2013. Geosynthetic Reinforced Soil Performance Testing—Axial Load Deformation Relationships. Report No. FHWA-HRT-13-066, Federal Highway Administration, McLean, VA.

Pierson, M.C., Parsons, R.L., Han, J., Brennan, J.J., 2009. Capacities and Deflections of Laterally Loaded Shafts behind an MSE Wall. Transportation Research Record, Journal of Transportation Research Board, 2116, Soil Mechanics 2009, pp. 62–69.

Pierson, M.C., Parsons, R.L., Han, J., Brennan, J.J., 2011. Laterally loaded shaft group capacities and deflections behind an MSE wall. J. Geotech. Geoenviron. Eng. ASCE. Rest. Va. 137 (10), 882–889.

Rowe, R.K., Skinner, G.D., 2001. Numerical analysis of geosynthetic reinforced retaining walls constructed on a layered soil foundation. Geotext. Geomemb. 19 (7), 387–412.

Skinner, G.D., Rowe, R.K., 2005. Design and behaviour of a geosynthetic reinforced retaining wall and bridge abutment on a yielding foundation. Geotext. Geomemb. 23 (3), 234–260.

Tatsuoka, F., Hirakawa, D., Nojiri, M., Aizawa, H., Nishikiori, H., Soma, R., Tateyama, M., Watanabe, K., 2009. A new type of integral bridge comprising geosynthetic-reinforced soil walls. Geosynth. Int. 16 (4), 301–326.

Tatsuoka, F., Tateyama, M., Uchimura, T., Koseki, J., 1997. Geosynthetic-reinforced soil retaining walls as important permanent structures: 1996–1997 Mercer Lecture. Geosynth. Int. 4 (2), 81–136.

Tensar International, 2012. Tensar® Uniaxial Geogrids for Soil Reinforcement, Technical Flyer.

Tognon, A.R., Rowe, R.K., Brachmen, R.W.I., 1999. Evaluation of side friction for a buried pipe testing facility. Geotext. Geomemb. 17, 193–212.

Wakai, A., Ugai, K., Matsuda, T., GOSE, S., 1996. Analysis of lateral displacement of a pile supported abutment constructed in a soft subsoil profile. Soils Found. 37 (4), 65–76.

Wu, J.T.H., Lee, K.Z.Z., Pham, T., 2006. Allowable bearing pressure of bridge sills on GRS abutments with flexible facing. J. Geotech. Geoenviron. Eng. 132 (7), 830–841.

Wu, J.T.H., Pham, T.Q., 2013. Load-carrying capacity and required reinforcement strength of closely spaced soil-geosynthetic composites. J. Geotech. Geoenviron. Eng. 139 (9), 1468–1476.

Yoo, C., 2001. Laboratory investigation of bearing capacity behavior of strip footing on geogrid-reinforced sand slope. Geotext. Geomemb. 19 (5), 279–298.

Please cite this article in press as: Xiao, C., et al., Experimental study on performance of geosynthetic-reinforced soil model walls on rigid foundations subjected to static footing loading, Geotextiles and Geomembranes (2015), http://dx.doi.org/10.1016/j.geotexmem.2015.06.001